Development and validation of a new MODIS snow-cover-extent product over China

Xiaohua Hao[1,2], Guanghui Huang[3,1,2], Zhaojun Zheng[4,5], Xingliang Sun[1,6], Wenzheng Ji[1], Hongyu Zhao[1], Jian Wang[1,2], Hongyi Li[1,2], Xiaoyan Wang[3]

[1]Heihe Remote Sensing Experimental Research Station, Northwest Institute of Eco-Environment and Resources, Chinese Academy of Sciences, Lanzhou 730000, China
[2]Key Laboratory of Remote Sensing of Gansu Province, Northwest Institute of Eco-Environment and Resources, Chinese Academy of Sciences, Lanzhou 730000, China
[3]College of Earth and Environmental Sciences, Lanzhou University, Lanzhou 730000, China
[4]National Satellite Meteorological Center, China Meteorological Administration, Beijing 100081, China
[5]Key Laboratory of Radiometric Calibration and Validation for Environmental satellites, China Meteorological Administration, Beijing 100081, China
[6]Engineering Laboratory for National Geographic State Monitoring, Lanzhou Jiaotong University, Lanzhou 730070, China

Correspondence to: Guanghui Huang (huanggh@lzu.edu.cn)

Abstract. Based on MOD09GA/MYD09GA surface reflectance data, a new MODIS snow-cover-extent (SCE) product from 2000 to 2020 over China has been produced by the Northwest Institute of Eco-Environment and Resources (NIEER), Chinese Academy of Sciences. The NIEER MODIS SCE product contains two preliminary clear-sky SCE datasets — Terra-MODIS and Aqua-MODIS SCE datasets, and a final daily cloud-gap-filled (CGF) SCE dataset. The formers are generated mainly through optimizing snow-cover discriminating rules over land-cover types, and the latter is produced after a series of gap-filling processes such as aggregating the two preliminary datasets, reducing cloud gaps with adjacent information in space and time, and eliminating all gaps with auxiliary data. The validation against 362 China Meteorological Administration (CMA) stations, shows during snow seasons the overall accuracies (OA) of the three datasets are larger than 93%, all of the omission errors (OE) are constrained within 9%, and all of the commission errors (CE) are constrained within 10%. Biases ranging from 0.98 to 1.02, to 1.03 demonstrate on a whole there are neither a significant overestimation nor a significant underestimation. Based on the same ground reference data, we found the new product's accuracies are obviously higher than standard MODIS snow products', especially for Aqua-MODIS and CGF SCE. For examples, compared with the CE of 23.78% that MYD10A1 product shows, the CE of the new Aqua-MODIS SCE dataset is 6.78%; the OA of the new CGF SCE dataset is up to 93.15%, versus 89.54% of MOD10A1F product and 84.36% of MYD10A1F product. Besides, as expected snow discrimination in forest areas is also improved significantly. An isolated validation at four forest CMA stations demonstrates the OA has increased by 3 – 10 percentage points, the OE has dropped by 1 – 8 percentage points, and the CE has dropped by 4 – 21 percentage points. Therefore, our product has virtually provided more reliable snow knowledge over China, and thereby can better serve for hydrological, climatic, environmental, and other related studies there.

1 Introduction

Snow is one of the most active elements on the land surface. Because of its unique properties of high shortwave reflectivity,
low longwave emissivity, and high phase-change latent heat, its covering may significantly alter the surface radiation budget,
exchanges of energy and moisture between the atmosphere and the surface, and thereby our climate and weather systems
(Henderson et al., 2018; Huang et al., 2019; Warren, 1982). In addition, seasonal snow is an important supply source,
providing precious freshwater for many arid and semi-arid regions (Li et al., 2019). Snow-cover-extent (SCE), therefore, is
an indispensable parameter in climatic, weather, hydrological, environmental, and other related studies.

With the development and progress of space technology, satellite remote sensing has become a primary option to monitor
snow-cover conditions on the Earth (Frei et al., 2012). In particular, as one of the most successful satellite missions, since
launched in 1999 the Moderate Resolution Imaging Spectroradiometer (MODIS) has been widely used to acquire SCE
information from regional to global scales (Gafurov, et al., 2016; Hall and Riggs, 2007; Hall et al., 2002; Muhammad and
Thapa, 2020). The reasons for this arise from: 1) MODIS is a multi-spectral sensor with a specific snow detecting band
around 1.64 μm; 2) features of nearly global coverage, double-satellite observations (Terra and Aqua), and suitable spatio-
temporal resolutions, also make it reasonable to acquire regional and global SCE.

The National Snow and Ice Data Center (NSIDC) routinely produces and continually updates the standard MODIS snow
products. Before the C6 version, there were only two sets of standard snow products — MOD10A1 and MYD10A1, which
provide conventional SCE information only under clear skies. Since there are abundant cloud-induced gaps in the products,
they in fact can not give the complete SCE knowledge. This is an obvious flaw for which reason the previous standard
products were criticized most (Liang et al., 2008). As such, among the latest C6.1 version that is released very recently
another two sets of new cloud-gap-filled (CGF) products, MOD10A1F and MYD10A1F, are introduced and generated (Hall
et al., 2019). But as of now, this update has not been completed yet, and these products are only available in some years.

In standard MOD10A1 and MYD10A1 products, the core is datasets of the Normalized Difference Snow Index (NDSI) that
is defined as,

$$NDSI = (b4 - b6)/(b4 + b6), \tag{1}$$

where b4 and b6 represent the reflectance of MODIS band 4 (0.55 μm) and band 6 (1.6 μm), respectively. The versions
before C5 adopted NDSI ≥ 0.4 as the threshold to discriminate snow-cover pixels and produced binary snow-cover datasets
(Riggs et al., 2006), whereas the versions after C6 only provide NDSI datasets, but indicate 0.1 as the new threshold (Riggs
et al., 2016). For clear skies, such a simple strategy is generally effective to distinguish snow cover because the snow has a
distinct NDSI characteristic relative to other common land covers. But there are also several appreciable shortcomings. First,
several studies (Hall and Riggs, 2007; Hao et al., 2019; Zhang et al., 2019) have shown that the optimal NDSI threshold may
vary with land-cover types, and using a fixed value for global products, regardless of 0.4 or 0.1, may lead to considerable
uncertainty. Second, standard MOD10A1 and MYD10A1 products often exhibit large errors in forest areas (Maurer et al.,
2003; Parajka et al., 2012; Poon and Valeo, 2006). For example, an evaluation conducted by Chen et al. (2014) indicates in

many forest regions of Northeast China the omission error or commission error may be up to 40%. Last but not the least, for snow discrimination theoretically using surface reflectance, is also more reasonable than using top-of-atmosphere (TOA) reflectance (what the standard products do), as the atmospheric contribution may virtually reduce the NDSI contrasts between snows and other land covers (Hall et al., 1995).

70 Although the new MOD10A1F and MYD10A1F are already able to give the complete daily snow information and thus would promote standard products' applications dramatically, there are still several deficiencies, as far as our experience. First, because of MODIS tradition, they are produced for Terra-MODIS and Aqua-MODIS separately, but many studies (Huang et al., 2014; Gao et al., 2010; Gafurov and Bardossy, 2009) have revealed that their synergy may be a better way to mitigate cloud influence. Second, their CGF mapping algorithm virtually only replaces cloud gaps in the current day with the

75 previous most-recent clear-sky observation (Hall et al., 2019). Implications indicated by the subsequent clear-sky observation or spatially adjacent observations are all neglected. Under many scenarios, this seems unreasonable. For example, the snowfalls often happen on cloudy days, and if only the previous clear-sky observation is used, these days would be very likely mistaken for snow-free days. More advanced algorithms appearing in these years often infer snow cover conditions beneath clouds comprehensively considering all available adjacent implications both in time and space (Huang et

80 al., 2018).

  Therefore, we decided to produce a new MODIS SCE product over China based on the Google Earth Engine (GEE) platform (Gorelick et al., 2017). Compared with the standard snow products, the following improvements are reached: 1) varying NDSI thresholds with land cover types are obtained by a volume of training data; 2) the approach that combines the Normalized Difference Vegetation Index (NDVI) and the Normalized Difference Forest Snow Index (NDFSI, Wang et al.,

85 2015; Wang et al., 2020), is adopted to improve snow discrimination in forest areas; 3) NDSI is computed using surface reflectance instead of TOA reflectance; 4) a Hidden Markov Random Field (HMRF) based gap-filling technique (Huang et al., 2018) is used to reduce cloud-induced gaps, which can assimilate temporally and spatially adjacent information simultaneously.

2 Data

90 **2.1 MODIS products**

  MODIS products we use as the input data to generate new SCE data include: MOD09GA, MYD09GA, and MCD12Q1. MOD09GA and MYD09GA are the standard land surface reflectance products that are derived from Terra MODIS and Aqua MODIS, respectively, after the so-called atmospheric correction. They provide the 500-m land surface reflectance from MODIS band 1 to band 7, as well as the mask information (e.g., cloud and water masks), and are our main inputting

95 data. MCD12Q1 is the Terra\Aqua composite land-cover-type product, providing the annual land-cover information that is generated according to the International Geosphere Biosphere Program (IGBP) land cover classification system. In the study,

it is another important input which is used to indicate the detailed land cover types. For all of the three products, the newest C6.1version is adopted.

2.2 Landsat-8 OLI snow maps and MOD09GA \ MYD09GA training samples

100 To refine the decision rules (will be elaborated in section 3), we must obtain the quality MOD09GA and MYD09GA training samples in advance. Toward this, two groups of Landsat-8 Operational Land Imager (OLI) snow maps across China during the 2013 – 2018 snow seasons (beginning on Nov. 1st through Mar. 31st of the next year) are produced here. The first group is derived from 1509 scenes of OLI images, which will be regarded as "true" values to acquire the Terra-MODIS training samples; and the second group comes from 1648 scenes of OLI images, which will be used to acquire the Aqua-MODIS

105 training samples. These snow maps are generated by the improved "SNOMAP" algorithm developed by Chen et al. (2020), and have a spatial resolution of 30-m. In every OLI snow map, there are only three classes — snow, snow-free, and cloud. Then 30-m snow maps will be aggregated within the 500-m spatial window to indicate whether the corresponding MOD09GA and MYD09GA pixel is covered by snow or not. Within a spatially and temporally (in the same day) collocated MOD09GA/MYD09GA pixel, if no less than 50% of OLI pixels are snow-covered, then it is a snow sample. If over 50% of

110 OLI pixels are snow-free, it is a snow-free sample. If the most of the OLI pixels are the class of cloud, it will be deemed as an invalid sample and is subsequently discarded. Of course, all of these must be done under the condition that the collocated MOD09GA/MYD09GA pixel is a clear pixel.

Finally, for the MOD09GA, totally 21.20 million snow samples and 17.66 million snow-free samples are obtained; for the MYD09GA, 12.05 million snow samples and 12.65 million snow-free samples are obtained in total. Note that it is necessary

115 to obtain the Terra-MODIS and Aqua-MODIS training samples separately, as MYD09GA band 6 is not the directly observing data (many sensor's detectors of this band have broken since the Aqua launch), but the restored data using the algorithm of Wang et al. (2006).

2.3 Auxiliary data

The auxiliary data we used include a snow-depth product generated from passive microwave satellite observations, a

120 reanalysis land surface temperature (LST) product, and a Digital Elevation Model (DEM) product.

The snow-depth product is available at http://data.tpdc.ac.cn, providing daily and 0.25 ° snow-depth data over China from 1979 to 2020, which is generated by Che et al. (2008) and Dai et al. (2015) through a combination of multiple satellites' passive-microwave observations. The reanalysis LST product is available on the GEE, providing daily and 0.25 ° LST data over China derived from ERA-5 global reanalysis (Munoz, 2019). The DEM product is one of the Shuttle Radar Topography

125 Mission (SRTM) DEM products with a resolution of 90-m and directly accessible on the GEE. To match with MODIS data, all of the three products had been resampled or aggregated into 500-m.

2.4 Ground snow-depth measurements

Daily ground snow-depth observations up to 362 stations from the China Meteorological Administration (CMA) since 2000 will be used to validate or assess all associated MODIS SCE products in the study. To ensure the qualities of the measurements, most CMA stations obey the following observing specifications: 1) snow-depth is measured manually in an open spot near the station using a professional ruler; 2) the measurements were conducted only when the fractional snow cover in the field of view is larger than 50%; 3) all observations were done at 8:00 Beijing time every morning.

At each station, the surface true condition, snow-cover or snow-free, is determined by the criterion proposed by Klein and Barnett (2003). That is, if measured snow-depth is $\geq$ 1-cm, it is covered by snow; else it will be snow-free. Because ground measurements are not limited by weather conditions, they are a better choice to independently validate all satellite-based SCE products.

3 Algorithm

3.1 Snow discrimination algorithm under clear-skies

Guided by the algorithm of MODIS standard snow products (Hall et al., 2002; Riggs et al., 2006; Riggs et al., 2016) and our motivations that are mentioned in section 1, we develop a new snow discrimination algorithm for clear-skies which is shown in Figure 1. Approximately, it is divided into three steps to determine snow-cover conditions under clear-skies from MODIS surface reflectance data. The first step is the preliminarily screening with the purpose of precluding the cases completely impossibly covered by snow. The second step provisionally determines snow-cover conditions over non-forest land-cover types using the optimized NDSI thresholds, and those over forest land-cover types through importing a new decision rule. Step three is the postprocessing based on surface temperature and DEM, which is designed to reverse those false snow pixels determined by the previous step into snow-free pixels.

3.1.1 Preliminarily screening

As mentioned just, the purpose of the preliminarily screening is to preclude the pixels that are impossibly covered by snow completely. Snow has the distinct spectral characteristic relative to other common land cover types. Generally, its reflectance is high in the visible spectrum, but rapidly drops in the infrared spectrum. As done by standard MODIS snow products (Riggs et al., 2006), we can use the combination of MODIS band 2 and 4 within the visible spectrum, and band 6 within the infrared spectrum to preliminarily screen out the pixels that must be snow-free, but keep all possible snow pixels (even with a very low possibility) for a further discrimination.

For that purpose, we investigate all available snow samples, and find for Terra-MODIS more than 99% of the snow samples are constrained in the condition of band 2 $\geq$ 0.15, band 4 $\geq$ 0.05, and band 6 $\leq$ 0.45. Therefore, the preliminarily screening rule of Terra-MODIS is adjusted into: all possible snow pixels must meet the condition of band 2 $\geq$ 0.15, band 4 $\geq$ 0.05, and

band 6 ≤ 0.45, and pixels that do not meet will be identified as snow-free immediately. Similarly, for Aqua-MODIS 99% of the snow samples are constrained in the condition of band 2 ≥ 0.12, band 4 ≥ 0.07, and band 6 ≤ 0.40. The preliminarily screening rule of Aqua-MODIS is set into: all possible snow pixels should meet this condition, and pixels that do not meet will be deemed as snow-free immediately.

3.1.2 Optimized NDSI thresholds over non-forest land cover types

NSDI threshold usually plays a key role in snow discrimination under clear-skies. Pixels whose NDSI value is ≥ this threshold will be identified as snow cover, and otherwise snow-free pixels are assigned. Therefore, here the optimal NSDI threshold is crucial.

To obtain optimal NDSI thresholds for snow discriminations over different land cover types, all of the training samples are first grouped according to their land cover types that are indicated by the MCD12Q1 products. With the type of "Barren or Sparsely Vegetated" as an example, the upper-left of Figure 2 presents the NDSI frequency distribution from Terra-MODIS training samples over this land cover, and the upper-right presents the fluctuation of overall accuracy (OA, see section 5 for details) with different NDSI thresholds. From the figure, one can see around the cross-point of snows and barren lands, the OA is highest (up to 98.34%) when the NDSI threshold = 0.08. Thus, 0.08 will be regarded as the optimal NDSI threshold for this land cover type. Similarly, the bottom-left and the bottom-right of Figure 2 present the NDSI frequency distribution and the fluctuation of OA derived from Aqua-MODIS training samples, respectively. It is apparent that for Aqua-MODIS the optimal NDSI threshold has changed to 0.06 and the highest OA is 95.20%.

Following the same philosophy, the optimal NDSI thresholds for the other seven land-cover types, such as "Grasslands", "Croplands", "Urban and Built-up Lands", etc., are also obtained and listed in Table 1, together with their corresponding OAs. One can see that over these land-cover types the OAs are all larger than 95%, which demonstrates the effectiveness of the new thresholds.

Table 1 Optimal NDSI thresholds over eight non-forest land-cover types

Land-cover types (IGBP)	NDSI thresholds (Terra)	Corresponding OA (%)	NDSI thresholds (Aqua)	Corresponding OA (%)
Barren or Sparsely Vegetated	0.08	98.34	0.06	95.20
Grasslands	0.03	97.57	-0.13	98.90
Croplands	0.17	98.89	0.26	99.02
Urban and Built-up Lands	0.17	98.44	-0.12	99.02
Cropland/Natural Vegetation	0.21	99.06	0.00	98.00
Closed Shrublands	0.52	97.19	0.14	99.89
Open Shrublands	0.06	99.94	0.03	99.77
Evergreen Broadleaf Forest	0.41	99.95	0.40	99.30

However, as we expected, only using the NDSI criterion seems not accurate enough to discriminate snow cover over those forest land-cover types, except the "Evergreen Broadleaf Forest" (due to its sparse distributions in China). For example, Figure 3 gives the Terra-MODIS NDSI frequency distribution and the fluctuation of OAs over the "Evergreen Needleleaf Forest". Obviously, here the commission error (CE, see section 5 for details) is very large (> 35%), and the OAs drop severely (< 76%). Therefore, for the remaining seven forest land-cover types, we will adopt a new decision rule as elaborated next.

3.1.3 Optimized NDVI-NDFSI decision-rules for forests

The study of Wang et al. (2015) had showed compared with NDSI, their so-called Normalized Difference Forest Snow Index (NDFSI, namely using band 2 to substitute band 4 in Eq. (1)) may be better for snow discrimination in forest areas. Our preliminary investigation reinforces this, and the improvement is, in particular, evident when using NDFSI in conjunction with NDVI (Wang et al., 2020).

Following their studies, NDVI in our study is divided into seven segments, and the optimal NDFSI at each NDVI segment will be computed with the highest OA as the object (similar to the acquirements of optimal NDSI thresholds). For a given pixel, if computed NDFSI is ≥ the threshold in its corresponding NDVI segment, it will be regarded as a snow pixel; else it will be a snow-free pixel. With "Deciduous Broadleaf Forest" as an example, Figure 4 shows the NDVI-NDFSI number-density scatterplot that is derived from Terra-MODIS training samples over this land cover, as well as computed optimal NDFSI thresholds at every NDVI segment. Here the OA of the new NDVI-NDFSI decision rule is 99.91%, versus 88.77% of the optimal NDSI threshold.

Using this approach, optimized NDVI-NDFSI decision rules for the left six forest land cover types are all determined. Table 2 and 3 give the detailed NDVI-depending NDFSI thresholds for Terra-MODIS and Aqua-MODIS, respectively. Besides these thresholds, the tables also give the OAs of the optimized NDVI-NDFSI decision rules in the second last column and the OAs of the optimal NDSI thresholds in the last column. We can see compared with optimal NDSI thresholds, optimized NDVI-NDFSI decision rules increase OAs greatly. Using the optimal NDSI thresholds, most OAs are ≤ 90%, whereas using the optimized NDVI-NDFSI decision rules, most OAs are ≥ 96%, in line with the accuracies of non-forest land cover types in Table 1.

Table 2 Optimized Terra-MODIS NDVI-NDFSI decision-rules for forest land-cover types (ENF: Evergreen Needleleaf Forests; DNF: Deciduous Needleleaf Forests; DBF: Deciduous Broadleaf Forests; PWS: Permanent Wetland Savannas)

Land-cover types (IGBP)	Terra-MODIS NDFSI thresholds							New OA[a] (%)	NDSI OA[b] (%)
	NDVI < 0.1	NDVI [-0.1,0)	NDVI [0.0,0.1)	NDVI [0.1,0.2)	NDVI [0.2,0.3)	NDVI [0.3,0.4)	NDVI ≥ 0.4		
ENF	-0.18	0.12	0.05	0.06	0.16	0.24	0.31	99.80	75.92

Land-cover types (IGBP)	NDVI < 0.1	NDVI [-0.1,0)	NDVI [0.0,0.1)	NDVI [0.1,0.2)	NDVI [0.2,0.3)	NDVI [0.3,0.4)	NDVI ≥ 0.4	New OA (%)	NDSI OA (%)
DNF	0.08	0.08	-0.11	-0.03	0.02	0.14	0.22	99.91	54.65
DBF	0.08	0.08	0.08	0.03	0.05	0.17	0.30	99.91	88.77
Mixed Forests	0.21	0.18	0.06	0.01	0.06	0.15	0.28	99.73	85.15
Woody Savannas	0.37	0.11	0.04	0.02	0.03	0.15	0.30	99.86	87.98
Savannas	0.29	0.13	0.07	0.06	0.04	0.24	0.36	99.91	86.43
PWS	0.50	0.19	0.12	0.17	0.31	0.35	0.35	85.53	81.42

New OA[a] refers to the OA of optimized NDVI-NDFSI decision-rules, and NDSI OA[b] refers to the OA of optimal NDSI thresholds.

Table 3 Optimized Aqua-MODIS NDVI-NDFSI decision-rules for forest land-cover types

Land-cover types (IGBP)	Aqua-MODIS NDFSI thresholds							New OA (%)	NDSI OA (%)
	NDVI < 0.1	NDVI [-0.1,0)	NDVI [0.0,0.1)	NDVI [0.1,0.2)	NDVI [0.2,0.3)	NDVI [0.3,0.4)	NDVI ≥ 0.4		
ENF	-0.09	-0.09	-0.28	-0.10	0.06	0.19	0.26	99.72	83.85
DNF	0.24	0.24	-0.24	-0.08	-0.07	0.07	0.23	99.62	88.11
DBF	-0.01	0.18	-0.03	-0.02	-0.02	0.16	0.40	99.91	93.30
Mixed Forests	0.28	-0.09	-0.10	-0.03	0.01	0.15	0.29	99.69	92.48
Woody Savannas	0.08	-0.01	-0.05	-0.05	-0.05	0.12	0.35	99.82	94.68
Savannas	0.20	0.01	-0.02	0.03	0.00	0.18	0.32	99.82	88.20
PWS	0.42	0.18	0.07	0.15	0.47	0.54	0.54	96.41	86.29

3.1.4 Postprocessing based on surface temperature and DEM

Ice clouds have similar optical properties to snows. From time to time pixels contaminated by broken ice clouds are mistaken
210   for snow pixels, which will lead to some false snow existences even in the tropics. Like standard MODIS products (Riggs et al., 2006), we also use the postprocessing based on surface temperature and DEM to reverse these snow pixels into snow-free pixels, but here ERA5 reanalysis LST (Munoz, 2019) is used rather than the brightness temperature from band 31. According to our previous investigation (Hao et al., 2021), for lowlands of DEM < 1300 m snow at the surface basically impossibly exists when their temperature is ≥ 275 K (2 degrees Celsius); but for highlands of DEM ≥ 1300 m, a higher
215   temperature threshold, 281 K (8 degrees Celsius), seems more appropriate due to possible existences of warm snow on highlands (Riggs et al., 2016). Thereby, if snow is detected in a pixel when its height < 1300 m and LST ≥ 275 K, this snow decision would be reversed to snow-free. If snow is detected in a pixel when its height ≥ 1300 m and LST ≥ 281 K, this snow decision would also be reversed to snow-free. Such a postprocessing is very effective to alleviate the problem of false snow detections which are often seen in summers or over south China (when and where snow is impossible).

3.3 Cloud-gap removing algorithm

Figure 5 describes the flow of the new cloud-gap removing algorithm we developed in the study. It can be divided into three steps. The first step is preliminarily excluding some cloud gaps by the synergy of Terra-MODIS and Aqua-MODIS; the second step is further filling gaps according to the implication of the nearby clear-sky pixels using Hidden Markov Random Field (HMRF) technique; and in step three all left gaps will be filled using the auxiliary passive microwave product.

3.2.1 Aggregation of Terra-MODIS and Aqua-MODIS

There may be different weather conditions when Terra and Aqua pass in one day, and their synergy can reduce cloud gaps approximately by $10 - 30\%$ over China (Huang et al., 2016). Thus, in the study, we will first aggregate the Terra-MODIS SCE and Aqua-MODIS SCE under clear-skies to preliminarily exclude some cloud gaps. The aggregating rule is in one day clear information no matter from Terra-MODIS or Aqua-MODIS will be reserved, and the cloud gap is kept still only if cloud existences are indicated by both.

3.3.2 Gap-filling based on the HMRF technique

For the aggregated SCE data, we will adopt the method based on the spatio-temporal Hidden Markov Random Field (HMRF) proposed by Huang et al. (2018) to further fill gaps. The core of this method is computing the total spatio-temporal "energy" (probability) of belonging to snow pixels or snow-free pixels at one specific gap, using

$$U(Snow) = U_{st} (Snow / N_s, N_t) \qquad (2)$$

$$U(Snow\text{-}free) = U_{st} (Snow\text{-}free / N_s, N_t) \qquad (3)$$

where U_{st} is the spatio-temporal neighbourhood energy function. N_s and N_t denote the spatial neighbourhood and temporal neighbourhood cantered with the gap, respectively.

Figure 6 illustrates our gap-filling process based on the HMRF technique. For a given gap, we will first calculate the $U(Snow)$ and $U(Snow\text{-}free)$ based on the 3 (row) $\times 3$ (column) $\times 3$ (day) spatio-temporal neighbourhood. If the $U(Snow)$ is > the $U(Snow\text{-}free)$, the gap will be classified as snow pixels; else it will be classified as snow-free pixels. If there are not sufficient valid pixels for calculating the $U(Snow)$ or $U(Snow\text{-}free)$, we will extend the spatio-temporal neighbourhood to 3 (row) $\times 3$ (column) $\times 5$ (day). If there are still not sufficient valid pixels, the spatio-temporal neighbourhood will expand into 5 (row) $\times 5$ (column) $\times 5$ (day). If the above tries all fail, the gap will be kept still.

The gap-filling technique based on the HMRF provides a rigorous analytical framework for integrating spatial and temporal contexts in an optimal manner, which is accurate and high-efficient for MODIS cloud-gaps filling (Huang et al., 2018). Our investigation shows this method can remove approximate 80% of the gaps in the aggregated data.

3.3.3 Eliminating residual gaps with auxiliary data

Although most cloud gaps have been filled after the above two processes, there are still a few exceptions. In this phase, we will use the auxiliary passive microwave snow-depth product provided by Che et al. (2008) to eliminate all remaining gaps. If collocated snow depth is ≥ 2-cm, then the gap will be assigned a snow pixel; else it will be a snow-free pixel (Hao et al., 2019).

4 Product

Using the new snow discrimination algorithm developed for clear-skies in section 3.1, we produce a new Terra-MODIS SCE dataset and a new Aqua-MODIS SCE dataset over China with MOD09GA and MYD09GA products as the main inputs. There are four classes of pixels in the new datasets, namely snow, snow-free, water body, and gap (see Figure 7). Because optical remote sensing is affected by clouds severely, there are often abundant gaps (up to 70%) in such clear-sky products, which limit their application to a very great extent.

Next, based on the two clear-sky datasets above, we produce a new CGF SCE dataset using the new cloud-gap removing algorithm developed in section 3.2. In the new dataset, all gaps have been removed and only three classes, snow, snow-free, and water body, are included (see Figure 7). Comparing with the first two datasets, this dataset undoubtedly has a wider application prospect.

The new Terra-MODIS, Aqua-MODIS, and CGF-MODIS SCE datasets together constitute the NIEER MODIS SCE product (Hao et al., 2021). It has a 500-m spatial resolution and a daily temporal resolution, providing the snow cover condition in the past two decades over China. An instance of snow coverage revealed by the product is presented in Figure 7.

5. Validation

A confusion matrix similar to Table 4 is used to validate or assess all associated MODIS SCE data in the study, in which the overall accuracy (OA) represents the percentage that snow and snow-free pixels are correctly classified, the producer's accuracy (PA, corresponding to the omission error, OE = 1 - PA) represents the percentage that real snow pixels are classified as such, the user's accuracy (UA, corresponding to the commission error, CE = 1- UA) represents the percentage that pixels classified as snow are also snow in reality. Because the Kappa coefficient have caused too much controversy recently (Pontius and Millones, 2011; Stehman and Foody, 2019), we no longer use it as an accuracy metric here. Meanwhile, to more directly show whether SCE is overestimated or underestimated and to what extent, a metric termed as "bias" is introduced. The bias, defined as the ratio of pixels classified as snow to real snow pixels (Hüsler et al., 2012; Wu et al., 2021), is a relative measure to detect overestimation (values > 1) or underestimation of snow (values < 1).

Table 4 Description of the confusion matrix used to validate or assess the associated SCE products (*SS*, *SN*, *NS*, and *NN* are the numbers in each case)

	MODIS SCE products	
	Snow	Non-snow
Reference	Snow	SS	SN
data	Non-snow	NS	NN

$$\text{OA}\,(\%) = \frac{SS + NN}{SS + SN + NS + NN} \times 100$$

$$\text{PA}\,(\%) = \frac{SS}{SS + SN} \times 100$$

$$\text{UA}\,(\%) = \frac{SS}{SS + NS} \times 100$$

$$\text{Bias} = \frac{SS + NS}{SS + SN} = \frac{\text{PA(\%)}}{\text{UA(\%)}}$$

Note that nominally 20-year and 362 stations' snow-depth measurements will be used as reference data to validate our product, but in fact validations are conducted only during the snow seasons at one station when the snow-cover days are ≥ 20, because otherwise, some accuracy metrics would become artificially high due to too many non-snow pixels in a mid-latitude region like China (Metsämäki, 2005).

5.1 Overview of the new product's accuracies

In Table 5, an overview is given of validation results for the new MODIS SCE product. We can see on a whole the two new clear-sky datasets are very accurate. For the Terra-MODIS SCE dataset, the OA, OE, and CE are 95.51%, 5.56% and 8.26%, respectively; and for the Aqua-MODIS SCE dataset, the OA, OE, and CE are 94.73%, 8.47%, and 6.78%, respectively. The former has a lower omission error, while the latter has a lower commission error. From the "bias" point of view, the Terra-MODIS dataset slightly overestimates snow cover, and the Aqua-MODIS dataset slightly underestimates snow cover. But from the specific values (1.03 and 0.98), the overestimation and underestimation are marginal. Comparatively speaking, the Aqua-MODIS dataset is inferior to the Terra-MODIS dataset. This is not surprising considering the problem of the Aqua-MODIS band 6 and the fact that CMA snow-depth measurement is only conducted in the mornings.

Although the CGF-MODIS SCE dataset is slightly worse than the two clear-sky datasets, there is not significant difference no matter from any accuracy metric. Here the OA, OE, and CE are 93.15%, 8.25% and 9.83%, respectively. Compared with the metrics shown above, the accuracy drops are basically within $1 - 2$ percentage points. Moreover, the bias of 1.02 also demonstrate an inconspicuous overestimation. Therefore, our cloud-gaps removing processes are effective and the accuracy may be sustained at a consistent level as the clear-sky datasets.

Table 5 Validation results of the new NIEER MODIS SCE product with reference to CMA ground measurements

	Terra-MODIS SCE dataset	Aqua-MODIS SCE dataset	CGF-MODIS SCE dataset

		Snow	Non-snow	Snow	Non-snow	Snow	Non-snow
CMA ground measurements	Snow	139664	8227	134324	12427	244005	21943
	Non-snow	12571	302759	9769	264397	26597	416366
OA (%)		95.51		94.73		93.15	
PA (%)/OE (%)		94.44		91.53		91.75	
UA (%)/CE (%)		91.74		93.22		90.17	
Bias		1.03		0.98		1.02	

5.2 The stability in time

To assess the stability of the NIEER MODIS SCE product in time, the accuracy metrics in every snow season since 2000 are calculated separately. Figure 8 presents the inter-annual fluctuation of these accuracy metrics. From the figure, we can see all of the three datasets have a similar fluctuation characteristic. They always perform a consistent high accuracy in one snow season, and a coincident low accuracy in another snow season. Such an accuracy fluctuation may be attributed to the different validation numbers available in different years caused by ground measurements.

The highest accuracy happens in the snow season of 2012, where the OEs of the three datasets are 2.84%, 5.76%, and 4.60%, and the CEs are 5.02%, 3.72%, and 6.01%. Meanwhile, the worse accuracy happens in the snow season of 2018, where the OEs of the three datasets are 9.49%, 12.91%, and 14.95%, and the CEs are 15.42%, 14.96%, and 17.15%. But except this snow season, the OEs and CEs in other seasons are all less than 15%. Relative to OE and CE (namely PA and UA), OA's fluctuations of the three datasets are smaller. The Terra-MODIS dataset fluctuates within 93% − 97%, the Aqua-MODIS dataset fluctuates within 93% − 96%, and the CGF-MODIS dataset fluctuates within 92% − 95%.

In addition, from the "bias" point of view, the values ranging from 0.94 to 1.07 demonstrate there are neither substantial overestimations nor substantial underestimations in all datasets and snow seasons. Therefore, on average the new product is stable in time and promising to better serve the climatic, hydrological, and other related studies in China (Huang et al., 2020).

5.3 The reliability in space

To clarify the new product's reliability in space, we calculate accuracies at each CMA station. With the Terra-MODIS SCE dataset as an example, Figure 9 presents the detailed accuracies. From the figure, we find, in spite of a very high accuracy seen at most stations, the errors may be relatively larger in the southwest of Northeast China and the north-eastern edges of Qinghai-Tibet Plateau. This can be attributed to their patchy snow-cover features and rugged terrains (Xiao et al., 2020), where Loess Plateau and Qinghai-Tibet Plateau rapidly transit toward Sichuan Basin and Northeast Plain, respectively. The Aqua-MODIS SCE dataset performs a very similar accuracy pattern like Figure 9, but slightly worse.

Figure 10 further details the accuracies of the CGF-MODIS SCE dataset at all stations. From the figure, we see that in North Xingjiang and the north of Northeast China where the snowpack is stable, the accuracy is high, whereas in the northeast of

Inner Mongolia, the northwest of North China, and the Qinghai-Tibet Plateau where snow may melt rapidly even in winter, the accuracy is relatively lower. Besides the propagated errors from the two original clear-sky SCE datasets, it is supposed that an unstable snowpack in warmer areas would result in another large uncertainty.

6 Discussion

6.1 Comparisons with standard MODIS products

Using the same ground reference data, we also evaluate the standard SCE data derived from the newest C6.1 MOD10A1, MYD10A1, MOD10A1F, and MYD10A1F products (see Table 6). Comparing the accuracy metrics listed here and those in Table 5, we can see that these products' accuracies are significantly lower than our product's. If ground measurements are seen as "true" values, MOD10A1 product's OE and CE are 7.22% and 12.97%, respectively, versus 5.56% and 8.26% of our Terra-MODIS dataset; MYD10A1 product's OE and CE are 13.78% and 23.78%, respectively, versus 8.47% and 6.78% of our Aqua-MODIS dataset. Our improvement is particularly significant for Aqua-MODIS SCE, where the CE is improved by over 17 percentage points. Besides, from the "bias" point of view, there are appreciable overestimations to snow cover in standard MOD10A1 and MYD10A1 products.

Note that here factual improvement may be much more obvious than shown by the accuracy metric of OA because there are a large number of non-snow pixels (far beyond snow pixels) in a mid-latitude region like China, which would pull up it dramatically. Although the new product's improvement in OA is within 1% relative to MOD10A1 products, in fact, the OE has decreased by 37% and the CE has decreased by 22%.

Table 6 Accuracies of SCE products derived from MOD10A1, MYD10A1, MOD10A1F, and MYD10A1F using the same ground measurements

Standard products	OA (%)	PA (%)	UA (%)	Bias
MOD10A1	95.47	92.78	87.03	1.07
MYD10A1	93.82	86.22	76.22	1.13
MOD10A1F	89.54	88.96	86.74	1.03
MYD10A1F	84.36	78.93	85.53	0.92

Due to possible wider application, the CGF products' comparison is emphasized here. Relative to the better standard product — MOD10A1F, our product's OA increases by nearly 4 percentage points, the OE drops from 11.04% to 8.43%, and the CE drops from 13.26% to 9.83%; relative to the worse standard product — MYD10A1F, the OA even increases by nearly 9 percentage points, the OE drops from 21.07% to 8.25%, and the CE drops from 14.47% to 9.83%. It is clear for the standard CGF products all of the OEs and CEs are larger than 10%, while for our product the OE and CE are both within 10%. Meanwhile, the two standard CGF products' biases are also further away from 1. Therefore, our improvement to CGF SCE

is obvious, too. Besides, comparing the two standard clear-sky products with the two standard CGF products, we find their cloud-gap removing strategy indeed lowers the accuracies dramatically.

6.2 Improvement in forest areas

To figure out the improvement in forest areas, the validations and comparisons at four forest CMA stations are isolated and listed in Table 7. From the table, one can see the OA increases by 3 − 10 percentage points, the OE drops by 1 − 8 percentage points, and the CE drops by 4 − 21 percentage points. As well, more significant improvements are seen for the Aqua-MODIS and the CGF SCE. For examples, the CE of the new Aqua-MODIS SCE dataset has already dropped to 9.62%, comparing with 30.13% of MYD10A1 product; the OA of the new CGF-MODIS dataset increases to 91.23%, compared with 81.79% of MOD10A1F product. Thus, the improvement of the new product in forest areas is also considerably significant, even more significant than in non-forest areas.

Table 7 Validation and comparison at four forest CMA stations

SCE products	OA (%)	PA (%)	UA (%)	Bias
Terra-MODIS SCE dataset	95.19	97.84	90.74	1.08
MOD10A1	92.48	96.62	86.01	1.12
Aqua-MODIS SCE dataset	94.18	97.77	90.38	1.08
MYD10A1	90.83	92.60	69.87	1.33
CGF-MODIS SCE dataset	91.23	93.39	92.12	1.02
MOD10A1F	81.79	85.95	84.10	1.02
MYD10A1F	82.78	89.53	83.12	1.07

Two more intuitional examples are shown in Figure 11. One is a typical forest area in Northeast China on Jan. 1st, 2018; another comes from southeast forest regions of Qinghai-Tibet Plateau on Feb. 1st, 2018. It is clear that the new MODIS-CGF SCE dataset agrees much better with the higher-resolution snow maps than the standard CGF product does. The standard MOD10A1F perceivably overestimates snow coverage in these forest areas.

Of course, the new product is far from perfect. In particular, the product's performance is limited severely by the cloud mask provided by standard MOD09GA/MYD09GA products, which is virtually caused by the cloud/snow confusion problem. On the one hand, some broken ice clouds are susceptible to being mistaken for snow pixels because of their similar optical properties, which will result in some artificial snow pixels in South China (although it has been mitigated largely compared with the standard MODIS snow products). On the other hand, snow pixels are also possibly mistaken for clouds, which will result in some omitted snow covers. During our validations or comparisons, we found this phenomenon is somewhat common in the edges of snow-cover areas and the forest areas of Northeast China.

7 Summary and outlook

In the study, we produce a new MODIS SCE product over China, which is committed to addressing currently known
370 problems of the standard snow products. Therefore, the optimal NDSI thresholds varying with land cover types are extracted, and the NDVI-NDFSI decision rules proposed by Wang et al. (2015) specific for snow discrimination in forest areas are optimized, by a number of training samples indicated by the higher-resolution snow maps from Landsat-8 OLI images. Meanwhile, to obtain a daily continuous cloud-free SCE dataset, the clear-sky snow SCE data from Terra-MODIS and Aqua-MODIS are aggregated first; an HMRF gap-filling technique, which can simultaneously assimilate temporally and
375 spatially neighbouring information, is imported second; finally, the residual gaps are all filled according to the implication given by an auxiliary passive microwave snow-depth dataset.

The new product is named the NIEER MODIS SCE product, which contains three individual datasets — the Terra-MODIS SCE dataset, the Aqua-MODIS SCE dataset, and the MODIS CGF SCE dataset. The first two provide the SCE knowledge under clear skies directly derived from the MODIS surface reflectance products, while the last provides daily and totally
380 continuous SCE knowledge.

The comprehensive validations against 362 CMA stations across China have revealed that our product is not only very accurate but also considerably stable in time and reliability in space. On a whole, there are neither any significant overestimations nor any significant underestimations in all datasets, and the cloud-gaps removing processes do not lower the SCE accuracy severely. Compared with SCE indicated by the standard MODIS snow products, our product's accuracies are
385 obviously higher, especially for the Aqua-MODIS and CGF SCE. Relative to MYD10A1 product, the CE drops 17 percentage points, from 23.78% to 6.78%. Relative to the better MOD10A1F CGF product, the OA increases by nearly 4 percentage points, from 89.54% to 93.15%. Meanwhile, as we expected the improvement in forest areas is also evident. If validations at forest stations are isolated, OA increases by 3 – 15 percentage points. Therefore, the new product has provided more reliable knowledge on snow coverage over China, and thereby will be a better choice for climatic, hydrological, and
390 other related studies there.

The problem of cloud/snow confusion may contribute to the largest uncertainty in the new product. There are many cases that snow pixels are mistaken for cloudy pixels or the opposite cases due to the inaccurate cloud mask provided by MOD09GA/MYD09GA products. In the future, we will consider further improving our product from this aspect.

Code and data availability

395 The new MODIS SCE product is available from the National Tibetan Plateau Data Center here: https://dx.doi.org/10.11888/Snow.tpdc.271387 (Hao et al., 2021). The code used to generate the product can be obtained from the authors without conditions.

Author contribution

XH, GH, and ZZ conceived and designed the study. XS, WJ and HZ developed the code and generated the product on GEE platform. GH and XH prepared the initial draft of the manuscript. All authors contributed to the data analysis, results' interpretation and validation, and revision of the manuscript.

Competing interests

The authors declare that they have no conflict of interest.

Acknowledgements

We would like to thank the China Meteorological Administration (CMA) for their reliable ground measurements, and the Google Earth Engine (GEE) for their high-quality services.

Financial support

This work was jointly supported by the National Natural Science Foundation of China (Grant No. 41971325; 42171322; 42171391), the National Key Research and Development Program of China (Grant No. 2019YFC1510503), and the Science & Technology Basic Resources Investigation Program of China (Grant No. 2017FY100502).

Review statement

This paper was edited by Hongkai Gao and reviewed by four anonymous referees.

References

Che, T., Li, X., Jin, R., Armstrong, R., and Zhang, T. J.: Snow depth derived from passive microwave remote-sensing data in China, Ann. Glaciol., 49, 145-154, doi:10.3189/172756408787814690, 2008.

Chen, S., Wang, X., Guo, H., Xie, P., Wang, J., and Hao, X.: A Conditional Probability Interpolation Method Based on a Space-Time Cube for MODIS Snow Cover Products Gap Filling, Remote Sens., 12, 3577, doi: 10.3390/rs12213577, 2020.

Chen, S. B., Yang, Q., Xie, H. J., Zhou, C., and Lu, P.: Time series of snow cover data of Northeast China (2004-2013), Acta Geographica Sinica, 69, 178-184, 2014.

Dai, L. Y., Che, T., and Ding, Y. J.: Inter-calibrating SMMR, SSM/I and SSMI/S data to improve the consistency of snow-depth products in China, Remote Sens., 7, 7212-7230, doi:10.3390/rs70607212, 2015.

Frei, A., Tedesco, M., Lee, S., Foster, J., Hall, D. K., Kelly, R., and Robinson, D. A.: A review of global satellite-derived snow products, Adv. Space Res., 50, 1007-1029, doi:10.1016/j.asr.2011.12.021, 2012.

Gafurov, A. and Bardossy, A.: Cloud removal methodology from MODIS snow cover product, Hydrol. Earth Syst. Sci., 13, 1361-1373, doi:10.5194/hess-13-1361-2009, 2009.

Gafurov, A., Ludtke, S., Unger-Shayesteh, K., Vorogushyn, S., Schone, T., Schmidt, S., Kalashnikova, O., and Merz, B.: MODSNOW-Tool: an operational tool for daily snow cover monitoring using MODIS data, Environ. Earth Sci., 75, Unsp 1078, doi:10.1007/S12665-016-5869-X, 2016.

Gao, Y., Xie, H. J., Yao, T. D., and Xue, C. S.: Integrated assessment on multi-temporal and multi-sensor combinations for reducing cloud obscuration of MODIS snow cover products of the Pacific Northwest USA, Remote Sens. Environ., 114, 1662-1675, doi:10.1016/j.rse.2010.02.017, 2010.

Gorelick, N., Hancher, M., Dixon, M., Ilyushchenko, S., Thau, D., and Moore, R.: Google Earth Engine: Planetary-scale geospatial analysis for everyone, Remote Sens. Environ., 202, 18-27, doi:10.1016/j.rse.2017.06.031, 2017.

Hall, D. K. and Riggs, G. A.: Accuracy assessment of the MODIS snow products, Hydrol. Process, 21, 1534-1547, doi:10.1002/hyp.6715, 2007.

Hall, D. K., Riggs, G. A., and Salomonson, V. V.: Development of Methods for Mapping Global Snow Cover Using Moderate Resolution Imaging Spectroradiometer Data, Remote Sens. Environ., 54, 127-140, doi:10.1016/0034-4257(95)00137-P, 1995.

Hall, D. K., Riggs, G. A., DiGirolamo, N. E., and Roman, M. O.: Evaluation of MODIS and VIIRS cloud-gap-filled snow-cover products for production of an Earth science data record, Hydrol. Earth Syst. Sci., 23, 5227-5241, doi:10.5194/hess-23-5227-2019, 2019.

Hall, D. K., Riggs, G. A., Salomonson, V. V., DiGirolamo, N. E., and Bayr, K. J.: MODIS snow-cover products, Remote Sens. Environ., 83, 181-194, doi:10.1016/S0034-4257(02)00095-0, 2002.

Hao, X. H., Huang, G. H., Zheng, Z. J., and Wang, J.: A new MODIS snow-cover-extent product over China (2000-2020), NTPDC, doi:10.11888/Snow.tpdc.271387.

Hao, X. H., Huang, G. H., Che, T., Ji, W. Z., Sun, X. L., Zhao, Q., Zhao, H. Y., Wang, J., Li, H. Y., and Yang, Q.: The NIEER AVHRR snow cover extent product over China − a long-term daily snow record for regional climate research, Earth Syst. Sci. Data, 13, 4711–4726, doi:10.5194/essd-13-4711-2021, 2021.

Hao, X. H., Luo, S. Q., Che, T., Wang, J., Li, H. Y., Dai, L. Y., Huang, X. D., and Feng, Q. S.: Accuracy assessment of four cloud-free snow cover products over the Qinghai-Tibetan Plateau, Int. J. Digit. Earth, 12, 375-393, doi:10.1080/17538947.2017.1421721, 2019.

Hao, X. H., Wang, J., and Li, H. Y.: Evaluation of the NDSI threshold value in mapping snow cover of MODIS — a case study of snow in the Middle Qilian Mountains, J. Glaciol. Geocryol., 30, 132-138, 2008.

Henderson, G. R., Peings, Y., Furtado, J. C., and Kushner, P. J.: Snow-atmosphere coupling in the Northern Hemisphere, Nat. Clim. Change, 8, 954–963, doi:10.1038/s41558-018-0295-6, 2018.

Huang, G. H., Li, X., Lu, N., Wang, X. F., and He, T.: A General Parameterization Scheme for the Estimation of Incident Photosynthetically Active Radiation Under Cloudy Skies, Ieee T. Geosci. Remote, 58, 6255-6265, doi:10.1109/Tgrs.2020.2976103, 2020.

Huang, G. H., Li, Z. Q., Li, X., Liang, S. L., Yang, K., Wang, D. D., and Zhang, Y.: Estimating surface solar irradiance from satellites: Past, present, and future perspectives, Remote Sens. Environ., 233, Unsp 111371, doi:10.1016/J.Rse.2019.111371, 2019.

Huang, X. D., Deng, J., Ma, X. F., Wang, Y. L., Feng, Q. S., Hao, X. H., and Liang, T. G.: Spatiotemporal dynamics of snow cover based on multi-source remote sensing data in China, The Cryosphere, 10, 2453-2463, doi:10.5194/tc-10-2453-2016, 2016.

465   Huang, X.D., Hao, X.H., Feng, Q.S., Wang, W., and Liang, T.G.: A new MODIS daily cloud free snow cover mapping algorithm on the Tibetan Plateau. Sci. Cold Arid Reg. 6, 116-123.doi: https://doi.org/10.3724/SP.J.1226.2014.00116, 2014.

Huang, Y., Liu, H. X., Yu, B. L., We, J. P., Kang, E. L., Xu, M., Wang, S. J., Klein, A., and Chen, Y. N.: Improving MODIS snow products with a HMRF-based spatio-temporal modelling technique in the Upper Rio Grande Basin, Remote Sens. Environ., 204, 568-582, doi:10.1016/j.rse.2017.10.001, 2018.

470   Hüsler, F., Jonas, T., Wunderle, S., and Albrecht, S.: Validation of a modified snow cover retrieval algorithm from historical 1-km AVHRR data over the European Alps, Remote Sens. Environ., 121, 497–515, doi:10.1016/j.rse.2012.02.018, 2012.

Klein, A. G. and Barnett, A. C.: Validation of daily MODIS snow cover maps of the Upper Rio Grande River Basin for the 2000-2001 snow year, Remote Sens. Environ., 86, 162-176, doi:10.1016/S0034-4257(03)00097-X, 2003.

Li, H. Y., Li, X., Yang, D. W., Wang, J., Gao, B., Pan, X. D., Zhang, Y. L., and Hao, X. H.: Tracing snowmelt paths in an

475   integrated hydrological model for understanding seasonal snowmelt contribution at basin scale, J. Geophys. Res.-Atmos., 124, 8874-8895, doi:10.1029/2019JD030760, 2019.

Liang, T. G., Huang, X. D., Wu, C. X., Liu, X. Y., Li, W. L., Guo, Z. G., and Ren, J. Z.: An application of MODIS data to snow cover monitoring in a pastoral area: A case study in Northern Xinjiang, China, Remote Sens. Environ., 112, 1514-1526, doi:10.1016/j.rse.2007.06.001, 2008.

480   Maurer, E. P., Rhoads, J. D., Dubayah, R. O., and Lettenmaier, D. P.: Evaluation of the snow-covered area data product from MODIS, Hydrol. Process, 17, 59-71, doi:10.1002/hyp.1193, 2003.

Metsämäki, S. J., Anttila, S. T., Markus, H. J., and Vepsalainen, J. M.: A feasible method for fractional snow cover mapping in boreal zone based on a reflectance model, Remote Sens. Environ., 95, 77-95, doi:10.1016/j.rse.2004.11.013, 2005.

Muhammad, S. and Thapa, A.: An improved Terra-Aqua MODIS snow cover and Randolph Glacier Inventory 6.0 combined

485   product (MOYDGL06*) for high-mountain Asia between 2002 and 2018, Earth Syst. Sci. Data, 12, 345-356, doi:10.5194/essd-12-345-2020, 2020.

Munoz, S. J.: ERA5-Land hourly data from 1981 to present, ECWMF, doi:10.2438/cds.e2161bac, 2019.

Parajka, J., Holko, L., Kostka, Z., and Bloschl, G.: MODIS snow cover mapping accuracy in a small mountain catchment - comparison between open and forest sites, Hydrol. Earth Syst. Sci., 16, 2365-2377, doi:10.5194/hess-16-2365-2012, 2012.

490   Pontius, R. G. and Millones, M.: Death to Kappa: birth of quantity disagreement and allocation disagreement for accuracy assessment, Int. J. Remote Sens., 32, 4407-4429, doi:10.1080/01431161.2011.552923, 2011.

Poon, S. K. M. and Valeo, C.: Investigation of the MODIS snow mapping algorithm during snowmelt in the northern boreal forest of Canada, Can. J. Remote Sens., 32, 254-267, doi:10.5589/M06-022, 2006.

Riggs, G.A., Hall, D.K., Roman, M.O.: MODIS snow products user guide for collection 6, http://modis-snow-

495   ice.gsfc.nasa.gov/?c=userguide, 2016.

Riggs, G.A., Hall, D.K., Salomonson, V.V.: MODIS Snow products user guide to collection 5, http://modis-snow-ice.gsfc.nasa.gov/?c=userguide, 2006.

Stehman, S. V. and Foody, G. M.: Key issues in rigorous accuracy assessment of land cover products, Remote Sens. Environ., 231, Unsp 111199, doi:10.1016/J.Rse.2019.05.018, 2019.

500 Wang, L. L., Qu, J. J., Xiong, X. X., Hao, X. J., Xie, Y., and Che, N. Z.: A new method for retrieving band 6 of Aqua MODIS, Ieee Geosci. Remote S., 3, 267-270, doi:10.1109/Lgrs.2006.869966, 2006.

Wang, X. Y., Chen, S. Y., and Wang, J.: An adaptive snow identification algorithm in the forests of Northeast China, Ieee J-Stars, 13, 5211-5222, doi:10.1109/Jstars.2020.3020168, 2020.

Wang, X. Y., Wang, J., Jiang, Z. Y., Li, H. Y., and Hao, X. H.: An effective method for snow-cover mapping of dense
505 coniferous forests in the upper Heihe River Basin using Landsat Operational Land Imager data, Remote Sens., 7, 17246-17257, doi:10.3390/rs71215882, 2015.

Warren, S. G.: Optical-Properties of Snow, Rev. Geophys., 20, 67-89, doi: 10.1029/Rg020i001p00067, 1982.

Wu, X., Naegeli K., Premier, V., Marin, C., Ma D. J., Wang J. P., and Wunderle, S. Evaluation of snow extent time series derived from Advanced Very High Resolution Radiometer global area coverage data (1982–2018) in the Hindu Kush
510 Himalayas, The Cryosphere, 15, 4261–4279, doi:10.5194/tc-15-4261-2021, 2021.

Xiao, P. F., Li, C. X., Zhu, L. J., Zhang, X. L., Ma, T. Y., and Feng, X. Z.: Multitemporal ensemble learning for snow cover extraction from high-spatial-resolution images in mountain areas, Int. J. Remote Sens., 41, 1668-1691, doi:10.1080/01431161.2019.1674458, 2020.

Zhang, H. B., Zhang, F., Zhang, G. Q., Che, T., Yan, W., Ye, M., and Ma, N.: Ground-based evaluation of MODIS snow
515 cover product V6 across China: Implications for the selection of NDSI threshold, Sci. Total Environ., 651, 2712-2726, doi:10.1016/j.scitotenv.2018.10.128, 2019.

520
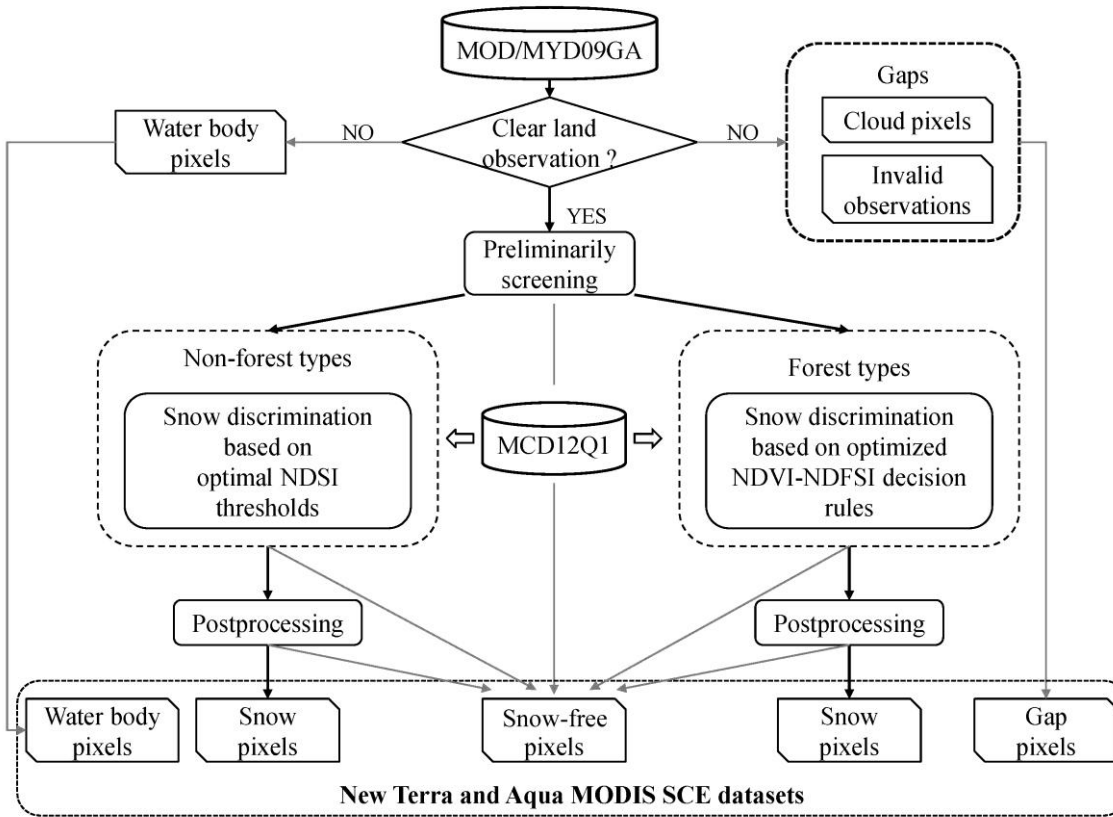
Figure 1: Flowchart of the new snow discrimination algorithm under clear-skies

525
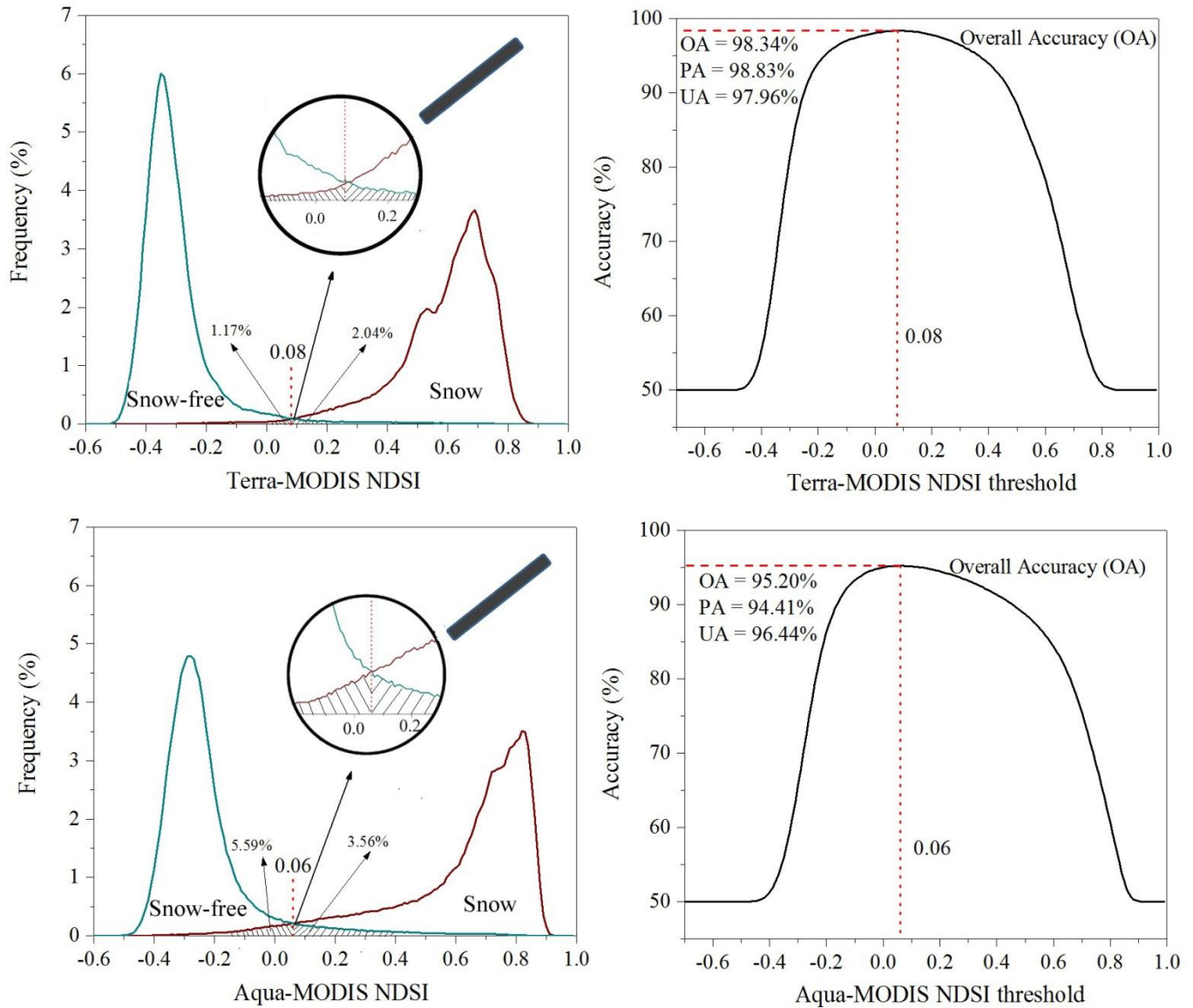
Figure 2: Optimal NDSI thresholds over the land cover type of "Barren or Sparsely Vegetated"
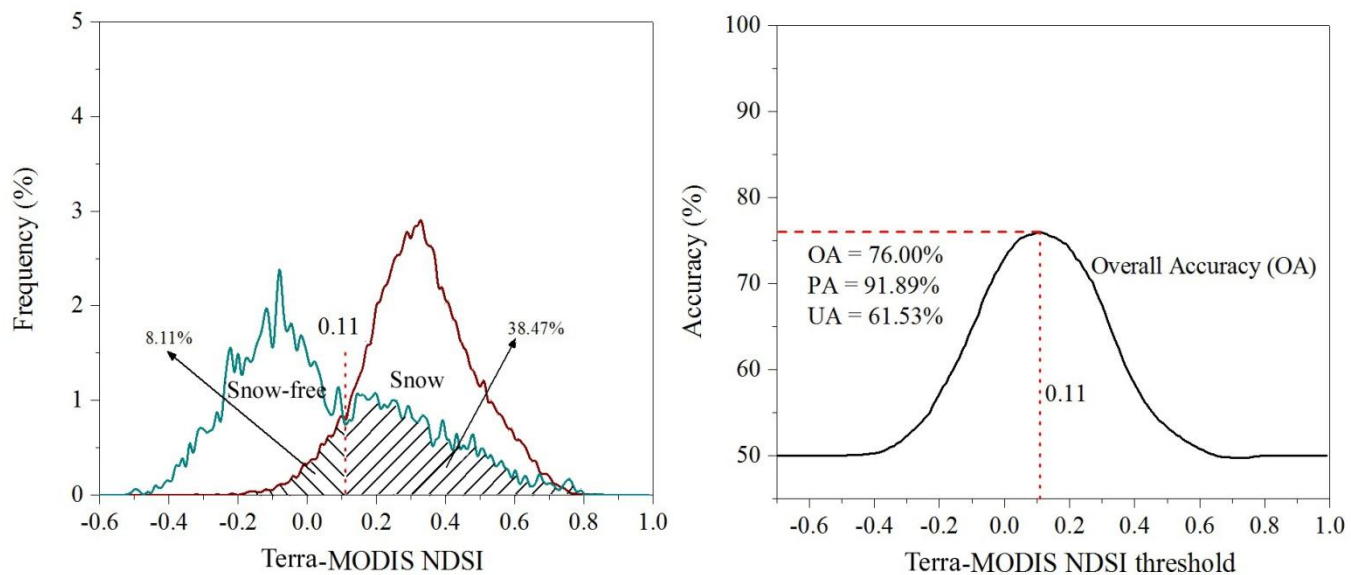
Figure 3: Optimal NDSI thresholds over the land cover type of "Evergreen Needleleaf Forest"
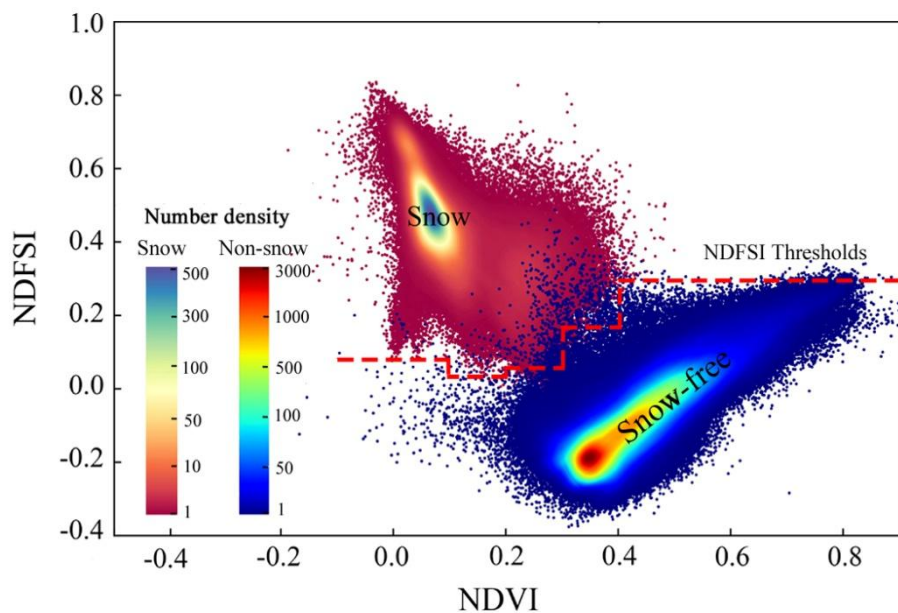
Figure 4: NDVI-NDFSI number-density scatterplot over "Deciduous Broadleaf Forest" from Terra-MODIS training samples
535 **(Colours represent the number-density within a 0.01×0.01 bin)**
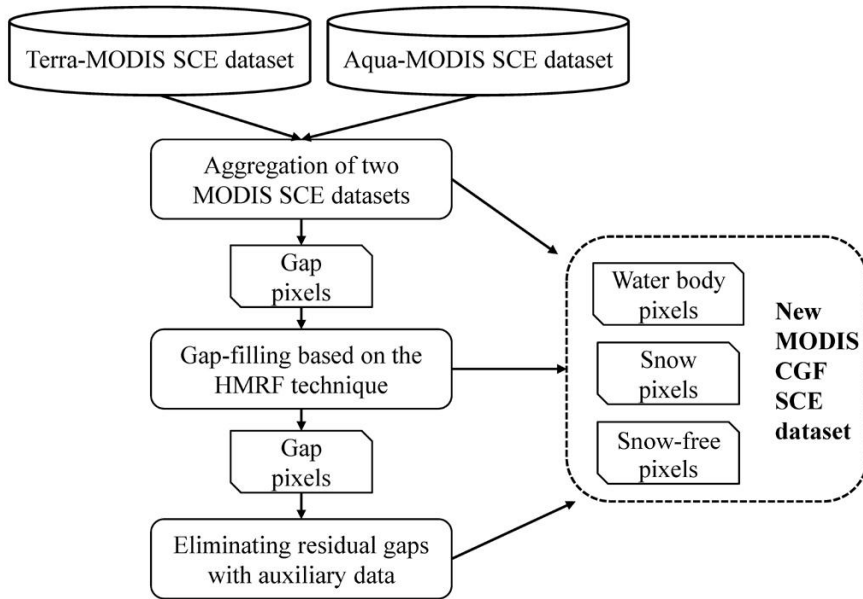
Figure 5: Flowchart of the new cloud-gap removing algorithm

540
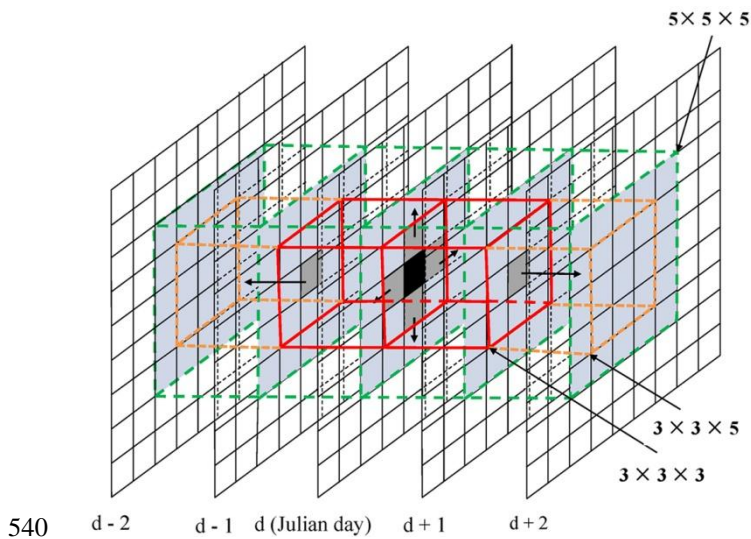
Figure 6: Diagram of the HMRF gap-filling process used in the study (Dark-grey represents high weight, and light-grey represents low weight)
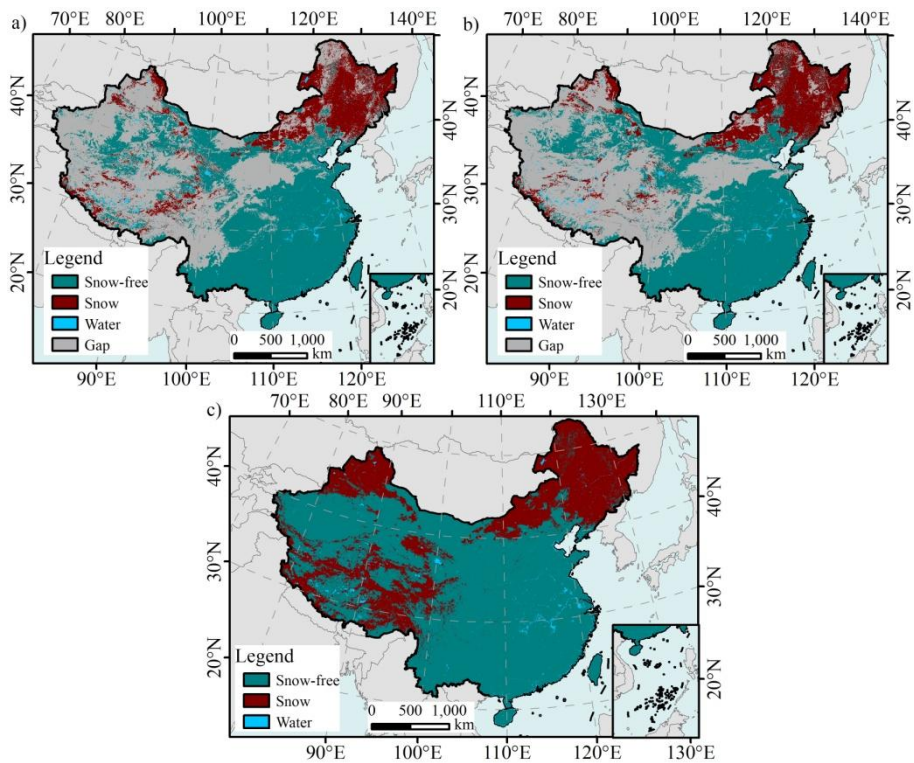
Figure 7: NIEER MODIS SCE product on Jan. 4, 2020: a) Terra-MODIS SCE dataset; b) Aqua-MODIS SCE dataset; c) CGF-MODIS SCE dataset
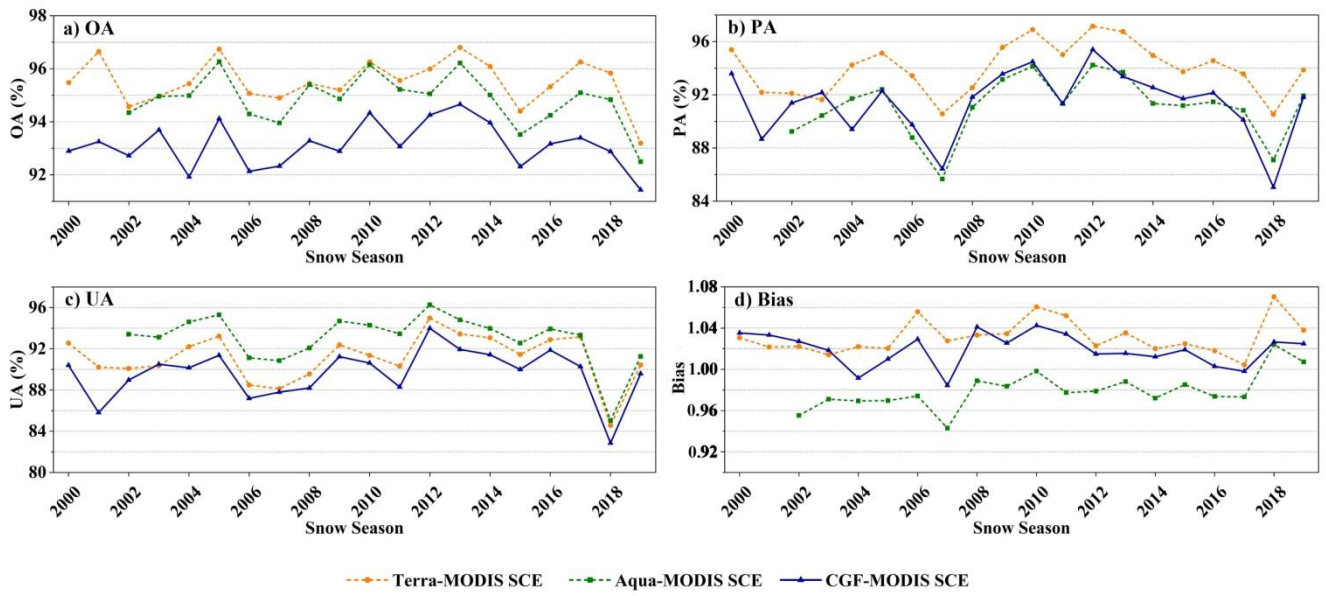
Figure 8: Annual accuracy metrics' fluctuation of the NIEER MODIS SCE product: a) OA; b) PA; c) UA; d) Bias

550
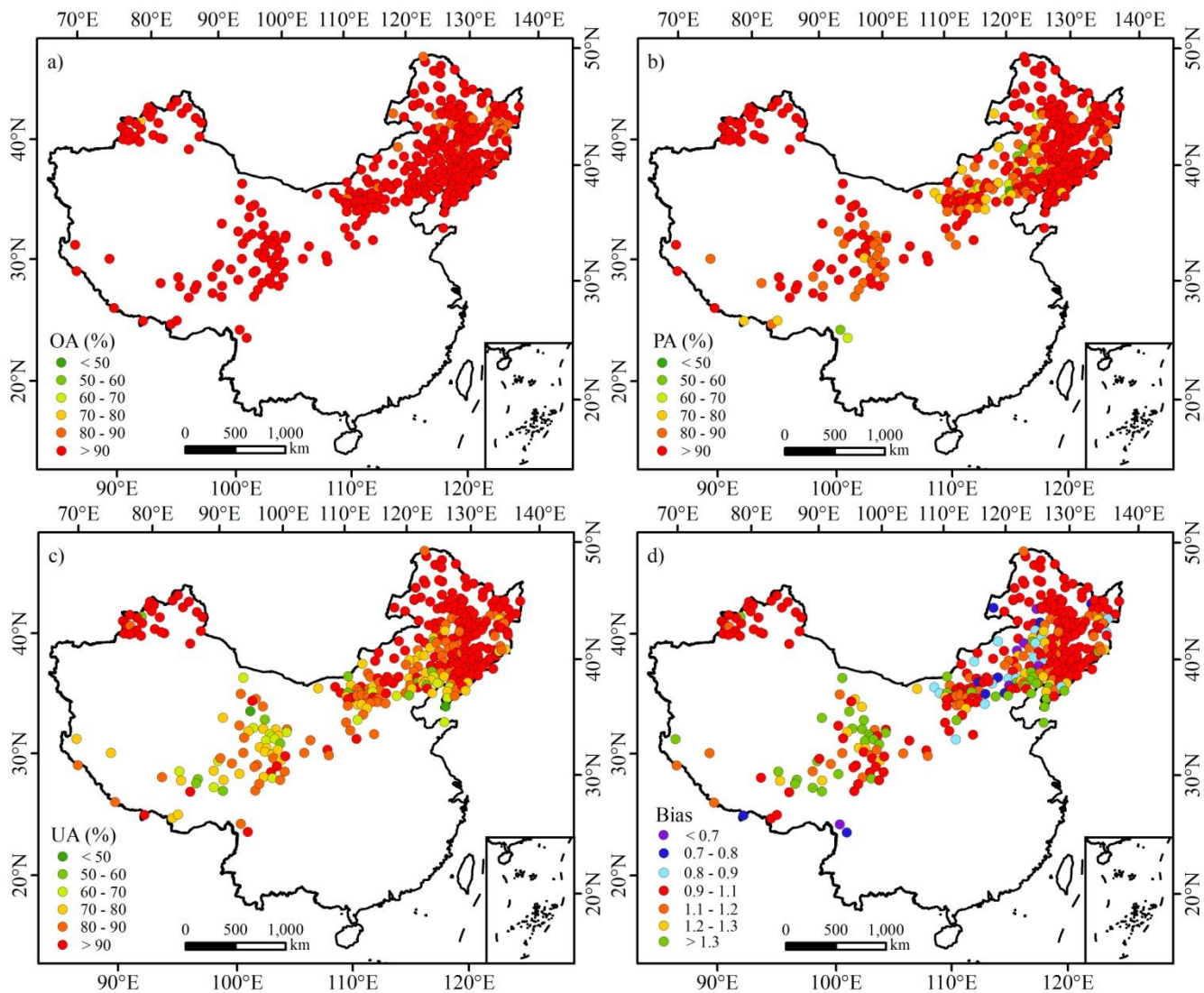
Figure 9: Accuracies of the Terra-MODIS SCE dataset at each CMA station: a) OA; b) PA; c) UA; d) Bias
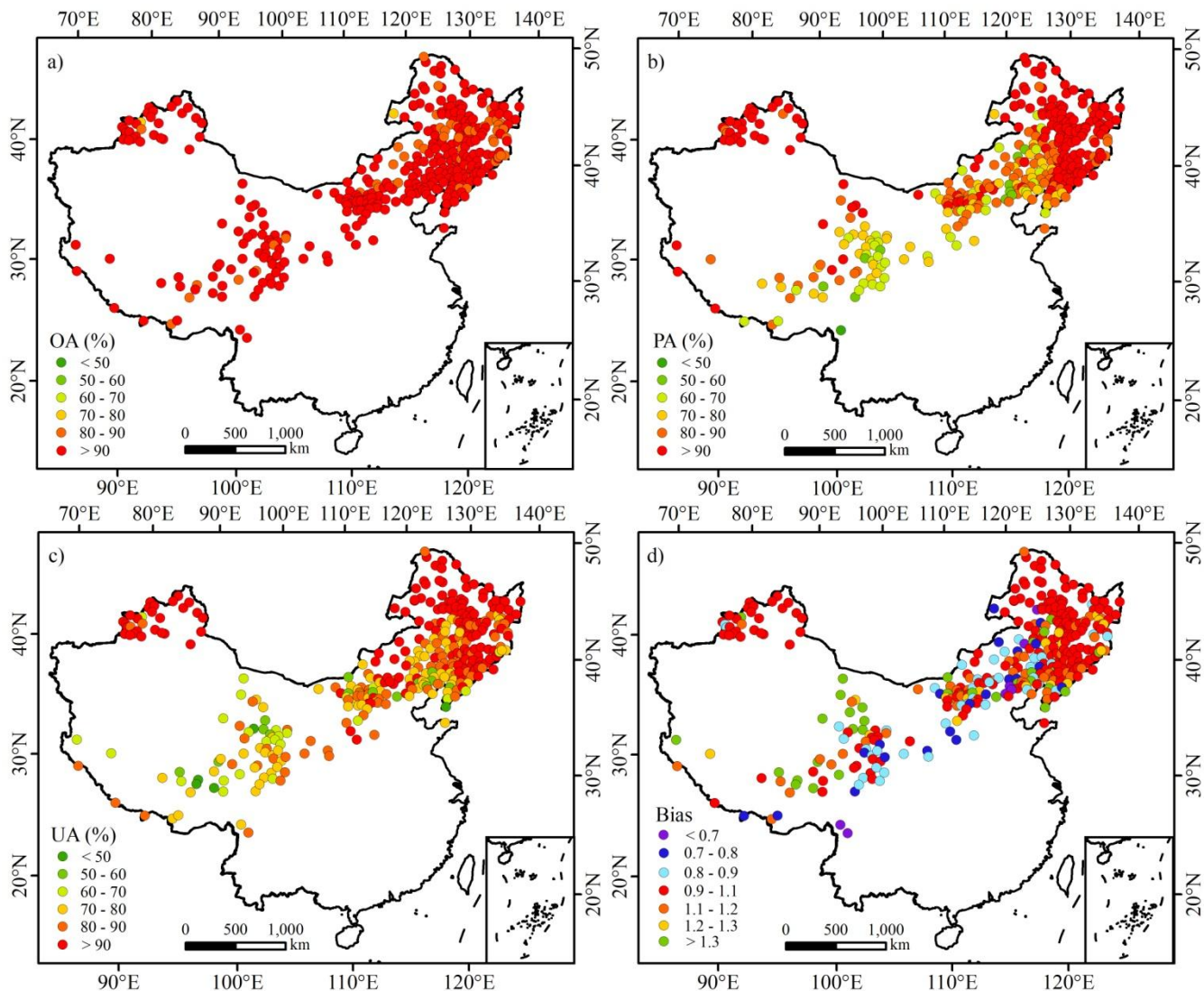
Figure 10: Accuracies of the CGF-MODIS SCE dataset at each CMA station: a) OA; b) PA; c) UA; d) Bias

555
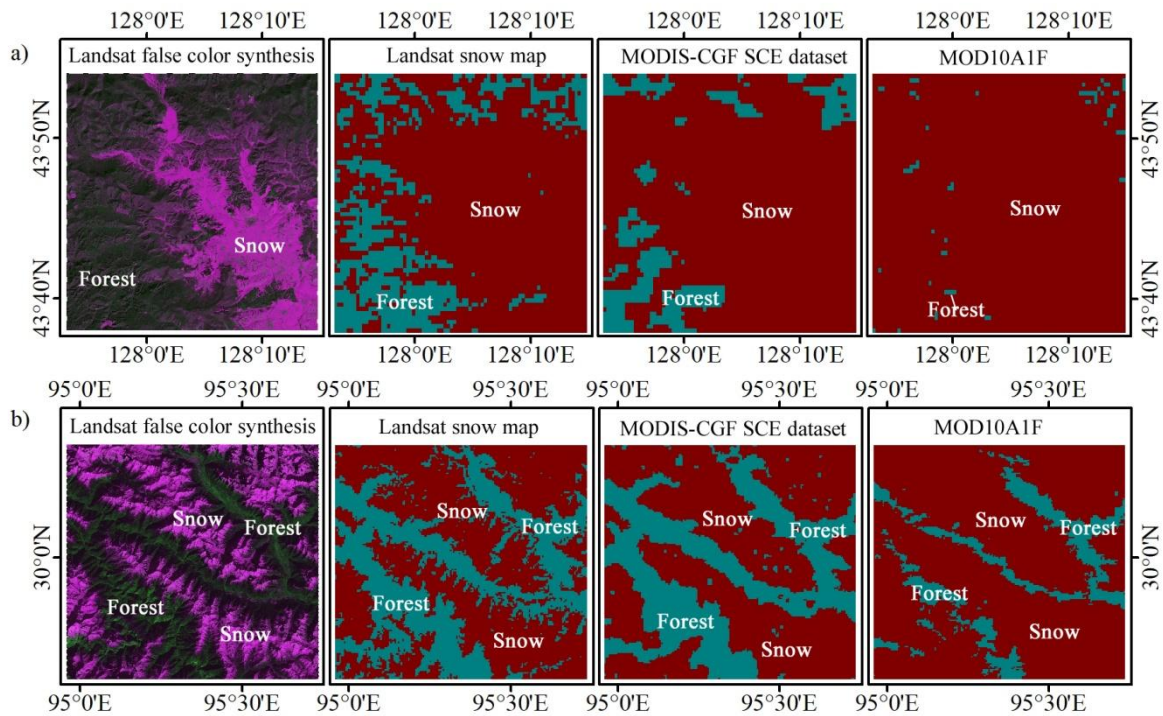
Figure 11: Intuitional improvements of CGF SCE in two representative forest areas: a) an example in Northeast China forest region; b) an example in Qinghai-Tibet Plateau forest region